Liquid-assisted pulsed laser ablation synthesized titanium ferrite nanoparticles: Structural, optical and magnetic properties

Abhishek Shukla[1], S. C. Singh[1], B. K. Pandey[1], K. N. Uttam[1], J. Shah[2], R. K. Kotnala[2], R. Gopal[1*]

[1]*Laser Spectroscopy and Nanomaterials Lab, Physics Department, University of Allahabad, Allahabad 211002, India*
[2]*CSIR-National Physical Laboratory (NPL), New Delhi 110012, India*

[*]Corresponding author. E-mail: profrgopal@gmail.com

ABSTRACT

Titanium ferrite nanoparticles (NPs) with controlled titanium to iron ratios (Ti/Fe) were synthesized using liquid-assisted pulsed laser ablation (LA-PLA) technique. Present manuscript describes effect of variation of Ti/Fe ratio in the target and the effect of laser pulse energy on size, shape, optical band gap, crystalline phase and magnetic properties of as-synthesized titanium ferrite NPs. UV-visible absorption, TEM and XRD investigations reveal that size of as-produced NPs decreases with the increase of Ti in the Ti/Fe targets used for ablation. Variation in laser pulse energy at a given Ti/Fe ratio has lesser dependence on size, shape and magnetic properties of produced NPs. Higher ferromagnetism with larger sized particles demonstrates dominance of bulk phenomenon over surface defects for the generation of ferromagnetic responsible spins. As-produced titanium ferrite nanomaterials may be used as promising magnetic recovery catalysts (MRCs). Copyright © 2015 VBRI Press.

Keywords: Laser ablation; titanium ferrite NPs; magnetic nanomaterials; laser induced coagulation.

Introduction

Liquid-Assisted Pulsed Laser Ablation (LA-PLA) is a quicker, purely green, and versatile method for the synthesis of metallic [**1, 2**], bimetallic [**3-5**] and metal oxide [**6, 7**] nanomaterials. Due to the unique photochemical and photophysical properties of nanoparticles over their bulk counterparts, nanoparticles are expected to be used as functional materials [**8**]. Titanium ferrites are widely being used as magnetically separable sorbent for elemental mercury capture from the flue gas of coal-fired power plants [**9**]. It is observed that the doping of Ti into the magnetite structure has a remarkable effect on promoting the decolorization of synthetic dyes, proving that titanomagnetite could be useful for environmental remediation [**10**]. As compared to the conventional nanopowder photocatalyst, TiO_2/Fe_2O_3 NPs can be used as a promising photocatalyst for the water purification at industrial scale and can be separated out by magnetic separation with the photocatalytic reaction and recycled easily [**11**]. Among the most promising composites, Fe–Ti oxide system is used as materials for spintronics, photocatalyst, gas sensors, solar battery elements etc. [**12, 13**]. Most of the nanocomposites are usually synthesized through co-precipitation or sol-gel methods [**14-17**]. Compared to other typically conventional methods, LA-PLA is a simple, quicker and purely green

approach that can synthesize nanomaterials of any solid target or powder in any reactive or non-reactive liquids [**18**]. It fascinates with several advantages over others synthesis methods including (a) large number of available ablation parameters to controlled size and shape of NPs, (b) capability to produce nanomaterials of desired chemical composition, and (c) NPs having surfaces free from chemical contamination. Composition of target material and laser pulse energy used in the ablation or post-irradiation of solution affect the size, shape, composition and degree of aggregation/ agglomeration [**19, 20**] which decides optical and ferromagnetic properties of produced nanomaterials [**21**].

Present manuscript deals with the LA-PLA synthesis of titanium ferrite NPs, where effects of variation in (i) laser pulse energy at constant Fe/Ti ratio and (ii) Fe/Ti ratio at constant laser pulse energy on structural, optical and magnetic properties of as produced nanomaterials are investigated.

Experimental

Preparation of targets

TiO_2 and Fe_2O_3 powders (purity 99.999 %, Sigma-Aldrich) were mixed in homogenizer pot for 45 min. followed by calcinations in a programmable furnace at 1000 ˚C with

2 ˚C/min heating and cooling rates. The process was repeated for three times to remove any undesired impurity in the powder. Calcinated mixtures of three different TiO_2 /Fe_2O_3 compositions were pelletized at 10 ton pressure followed by annealing at 1000 ˚C to harden them for laser ablation.

Fig. 1. Digital photographs of prepared powder and pellets.

   Fig.1. represents photographs of calcinated powder and pellet before and after annealing. Three such pellets made with the addition of 80, 40 and 8 mg of TiO_2 into 1.6 g of Fe_2O_3 were assigned as P1, P2 and P3 respectively.

Synthesis of titanium ferrite NPs

Titanium ferrite NPs were synthesized using experimental setup shown in **Fig. 2**. Pellet, placed at the bottom of glass vessel containing 20 ml of double distilled water, was allowed to irradiate with focused output of 1064 nm from pulsed Nd:YAG laser (Spectra Physics, INDI Series, USA) operating at 40-60 mJ/pulse energy, 10 ns pulse width, 10 Hz rep. rate for one hour. Thus obtained colloidal solution of NPs was post-irradiated for one hour using same laser parameters. Two sets of experiments, ablation followed by post-irradiation of (i) P1, P2 and P3 targets using 40 mJ/pulse energy, and (ii) P2 target with varying laser pulse energy, were performed in order to investigate the effects of variation in target composition at constant laser parameter and laser pulse energy at given target parameters, respectively.
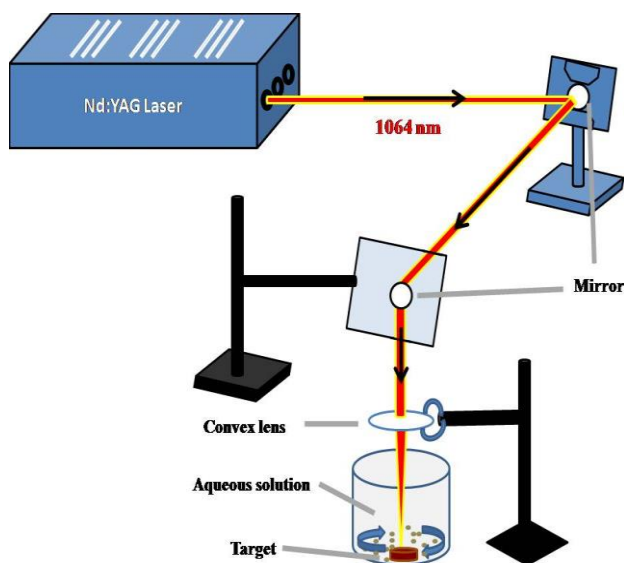

Fig. 2. Experimental setup of LA-PLA.

Characterization of NPs

As obtained colloidal solution of NPs were employed for UV-visible absorption measurements using Perkin Elmer Lambda-35 double beam spectrophotometer. A drop of solution was poured on carbon coated copper grid and dried for particles size and distribution measurements using JEOL-JEM2000FX Transmission Electron Microscope attached with EDAX. For crystallographic investigations, colloidal solutions were dried by placing them inside the hot air oven at about 60 ^{0}C. The diffractograms were recorded employing Cu K_α line (λ=1.054 Å) from Philips X'PERT X-ray diffractometer operating at 40 kV. Magnetic measurements of powder samples were carried out using Lakeshore Vibrating Sample Magnetometer at room temperature.

Results and discussion

Structural and compositional investigation of as synthesized NPs

Fig. 3 (**a**) illustrates XRD patterns of titanium ferrite NPs with varying TiO_2 and Fe_2O_3 composition, while **Fig. 3** (**b**) depicts diffraction patterns of titanium ferrite NPs samples obtained by LA-PLA of P2 pellet at different laser energies.
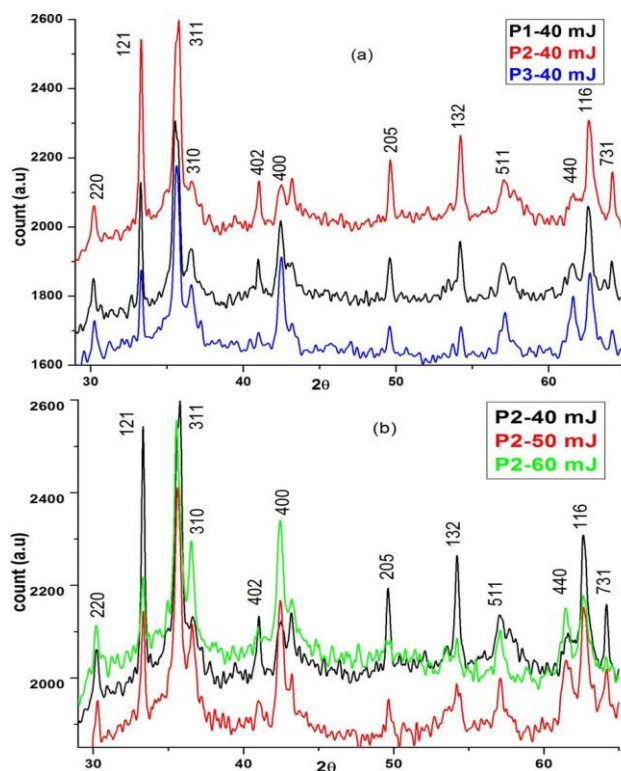

Fig. 3. XRD pattern of titanium ferrite NPs for (a) fixed 40 mJ laser energy with variation of TiO_2 weight in % and (b) fixed TiO_2 weight (%) with 40, 50 and 60 mJ laser energy.

The diffraction peaks observed at 2θ = 30.27˚, 35.58˚ and 57.07˚ corresponds (220), (311) and (511) respectively, planes of titanomaghemite ($Fe_{.23}$ ($Fe_{1.95}Ti_{0.42}$) O_4) with cubic primitive lattice parameter a = 8.34Å (JCPDS NO. 84-1595). The XRD peaks at 2θ = 36.56˚, 41.06˚, 49.65˚,

and 62.61˚ correspond diffraction from (310), (402), (205), and (116) respectively, planes of pseudobrookite ($TiFe_2O_5$) phase with orthorhombic and end-centered structures having lattice parameters, a = 9.700 Å, b = 3.720 Å, c = 9.930 Å (JCPDS NO. 73-1631). Besides these diffraction peaks at 2θ = 33.25˚ and 54.18˚ correspond diffraction from (121) and (132) planes respectively of hematite (Fe_2O_3) structure with hexagonal and rhomb-centered with lattice parameters, a = 5.420 Å, α = 55.120 (JCPDS-85-0599). XRD peaks at 2θ = 42.56˚ and 61.48˚ resemble ulvoespinel ($TiFe_2O_4$) structure corresponding to (400) and (440) respectively planes with cubic, face-centered lattice parameters, a = 8.509 Å, (JCPDS- 71-1141). Peak at 2θ = 64.25˚ corresponds diffraction from (731) plane of Ti_3Fe_3O phase having cubic, face-centered with lattice parameter a = 11.14 Å, (JCPDS-75-0397). Formation of TiO_2/Fe_2O_3 nanocomposite is possible due to similar ionic radii of Ti^{4+} (0.68 Å) and Fe^{3+} (0.64 Å) [22].

The particle size is estimated from XRD peaks using Scherrer's formula-

$$D = \frac{K\lambda}{\beta cos\theta}$$

where, constant K = 0.97, λ = 1.5406 Å is the wavelength of X-ray line used and β is the full width at half maximum. Average crystalline size is estimated using five most intense peaks from the diffraction data of each sample. The average crystalline size of the samples from P1 to P3 is shown in **Table. 1**.

Table. 1. Parameters used in synthesis of titanium ferrite NPs.

S.No	Sample	Band gap (eV)		Size (nm)		Mr (emu/g)	Ms (emu/g)	Hc (Oe)
		Laser ablation	Post irradiation	XRD	TEM			
1.	P1 40	3.89	2.15	22.36	15.30	2.08	10.00	229.95
2.	P2 40	3.80	2.05	23.40	18.00	2.62	14.89	179.87
3.	P2 50	2.43	2.29	23.53	9.33	2.86	13.27	221.92
4.	P2 60	2.56	2.06	25.21	16.01	2.68	13.20	208.40
5.	P3 40	3.71	2.20	27.02	18.70	4.32	22.30	216.51

With the increase in TiO_2 concentration from 0.5 % to 5 % in the target used for ablation, decreases the size of as produced NPs from 27 to 22 nm. This variation in crystalline size may be due to the charge imbalance between titanium and iron. With the decrease in laser pulse energy from 60 to 40 mJ/pulse to ablate the fixed Ti/Fe target composition, the size of NPs decreases from 25 to 23 nm.

Optical property measurements of as synthesized NPs

UV–vis absorption spectra of as synthesized titanium ferrite NPs colloidal solutions produced by LA-PLA in double distilled water with 40 mJ/pulse energy are shown in **Fig. 4**. Absorption spectra shown in **Fig. 4 (a)** correspond to as produced NPs with variation in TiO_2 composition in target, while those presented in **Fig. 4 (b)** correspond to samples produced after 1 hour post irradiation treatment.
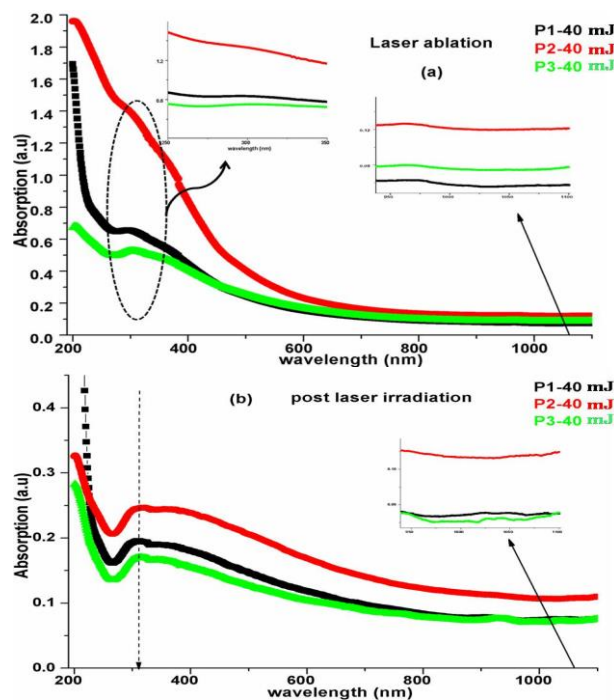

Fig. 4. UV visible absorption spectra of colloidal NPs in DDW at fixed energy of 40 mJ/pulse with (a) laser ablation and (b) post irradiation.

UV-visible absorption spectra of all samples those are recorded before as well as after post-irradiation treatment have absorption hump near ~310 nm, which is characteristic absorption peak of titanium ferrite NPs. [23]. Absorption peak in deep UV region near 200 nm is consequence of electronic transitions from inner shell electrons of titanium and iron [24, 25]. Position and width of characteristic absorption peak determine the size and distribution of NPs, while absorbance of deep UV peak tells about particle concentration in colloidal solution. Absorption peak at 310 nm as shown in inset of **Fig. 4 (a)** shifts towards shorter wavelength side with the increase of TiO_2 weight percentage in target, which affirms decrease in particle size. Increase of TiO_2 composition in the target enhances its melting/evaporation point and hence decreases per pulse vaporized mass from target surface that consequences decrease in particle size and number of particles in solution. Highest percentage of TiO_2 in target P1 produces smallest size of titanium ferrite NPs, while that of lowest percentage of TiO_2 in target P3 corresponds to maximum size. Largest size and highest yield of NPs produced by LA-PLA of target P3, increases particle-particle interaction and hence larger degree of aggregation/agglomeration which results their gravitational settlement on the bottom of ablation vessel. Though particle yield corresponding to P3 is highest due to its minimum ablation threshold but absorbance is least on the account of reduced number of particles in suspension. It means that by varying the Ti/Fe ratio in target one can tune size of LA-PLA produced NPs.

For the post-irradiation treatments, the target is removed and solution is irradiated under continuous stirring. Absorbance at 1064 nm decides interaction cross section between particles and laser beam that results any modification in size and shape of particles, and laser

induced coagulation (LIC) process. Absorbance at 1064 nm is maximum {inset (**Fig. 4** (**a**)} for the colloidal solution produced with PLA of target P2, which results enhancement in absorbance and reduction in its absorbance at 310 nm.

The direct band gap E_g of NPs of Ti/Fe estimated from tauc plot is larger in higher titanium concentration target. After post-irradiation treatments, change in band gap and hence change in the size of particles is maximum for the sample P2, which is also evidenced from the maximum absorbance of as-produced solution at 1064 nm {inset (**Fig. 4** (**a**)}. Here post-irradiation treatment increases the size of particle and this increase is maxima for the sample corresponding to target P2, which may be due to the LIC process. In LIC process, electrons in the particle oscillate in the field of laser pulse to make them as dipole. Dipole-dipole interaction between different particles is the cause of coagulation to increase in particle size. Post-irradiation treatment increases width of UV-visible absorption peak at 310 nm, which demonstrates that LIC process increases size distribution of particles.

UV–vis absorption spectrum of as synthesized NPs colloidal solutions produced with LA-PLA of pellet P2 with varying laser pulse energy between 60 mJ to 40 mJ/pulse are shown in **Fig. 5**.
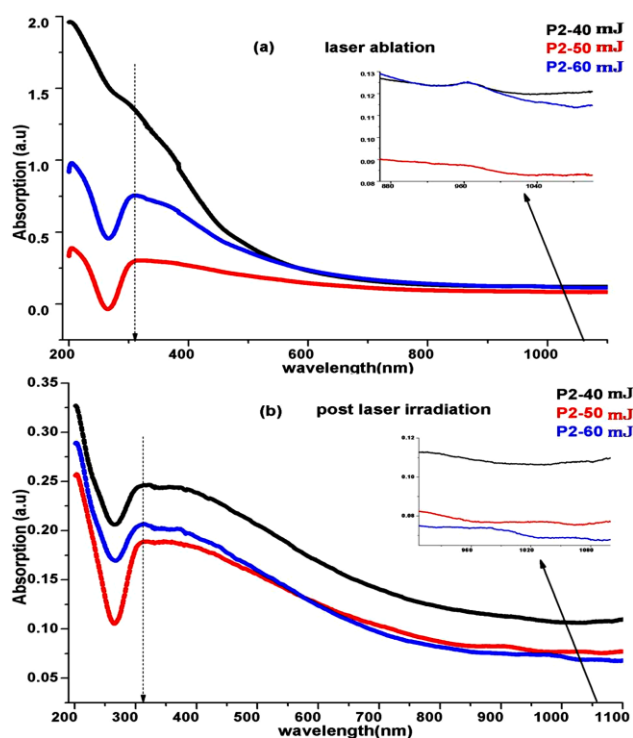

Fig. 5. UV visible absorption spectra of P2 with varied energy 40, 50 and 60 mJ of (a) laser ablation (1 hour) (b) post irradiation (1 hour) colloidal NPs in DDW.

Decrease in laser pulse energy decreases per pulse ablated mass from target surface, and hence decrease of particle size and yield. Smaller optical absorbance at 310 nm for the solutions produced with PLA of P2 target with 50 and 60 mJ/pulse energies, demonstrates aggregation/agglomeration followed by gravitational settlement of particles at the bottom of ablation vessel.

With the increase of laser pulse energy, absorption peak near 310 nm shows red shift, which demonstrates increase in particle size. Higher laser pulse energy corresponds higher particle yield in the solution that results increased particle-particle interaction followed by aggregation/agglomeration and gravitational settlement. Decrease in particle concentration in the solution corresponding to larger pulse energy reduces absorbance as shown in **Fig. 5** (**a**). Width of the optical absorbance at 310 nm increases with the increase of laser pulse energy that demonstrates larger size distribution of particles corresponding to higher pulse energy. UV-visible absorption spectra of post-irradiated samples, shown in **Fig. 5** (**b**), demonstrate decrease in absorbance as well as peak width compared to non irradiated samples. Decrease in peak width reveals reduced particle size distribution as a consequence of laser induced thermal evaporation of surface atoms of larger size particles to make them smaller sized [**26**], while absorbance decreases due to the LIC process. Thermal evaporation and LIC processes, measured from change in width and absorbance respectively, is maximum for solution produced with 40 mJ/pulse energy due to the maximum absorbance at 1064 nm {inset (**Fig. 5** (**a**)}. Post-irradiation of PLA produced colloidal solution causes increase in particles size and decrease in particle size distribution.

TEM characterization

Fig. 6 shows TEM micrographs and corresponding EDX patterns of titanium ferrite NPs obtained from laser ablation followed by post-irradiation of P1, P2 and P3 pellets with 40 mJ/ pulse energy.
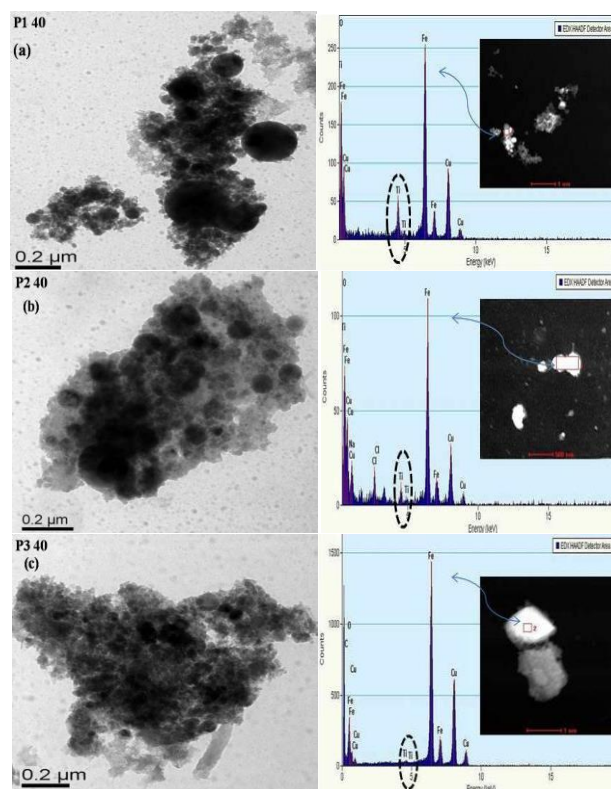

Fig. 6. (**a-c**) TEM micrographs with their EDX spectrum of samples P1, P2 and P3 synthesized at 40 mJ energy.

It is evident from micrographs that particles are spherical in shape and smaller particles have tendency to form bigger clusters [27]. Micrographs illustrate that with the increase of titanium dioxide concentration in the pellet, yield and degree of aggregation decreases which is in accordance with the results obtained from optical investigation. It is interesting to note that with the increase of Ti concentration from 0.5 % to 5 %, degree of spherical like structure formation increases, while particles size decreases from 18.70 to 15.30 nm as shown in **Table. 1**. This demonstrates that Ti is incorporated with Fe to form spherical like structures. Mostly all samples show agglomeration due to highly magnetic behavior of titanium ferrite NPs. Furthermore the particle diameter of NPs are about 45, 75 and 31 nm for sample P1, P2 and P3, respectively near the agglomerated region.

Energy Dispersive X-Ray spectroscopy (EDX) is analytical technique used for elemental analysis or chemical characterization of sample. Here EDX spectrum clearly depicts that intensity of Ti line decreases with the decrease in Ti concentration in target as shown in dotted circle in **Fig. 6**, which demonstrates presence of Ti in titanium ferrite NPs and inherence capability of LA-PLA to attain stoichiometry of mother target. Other elements like Cu appears in EDX spectrum due to deposition of colloidal solution on the carbon coated copper grid. **Fig. 7** (**a-c**) represents particle size distributions with corresponding SAED pattern (inset of **Fig. 7**) of samples P1, P2 and P3.
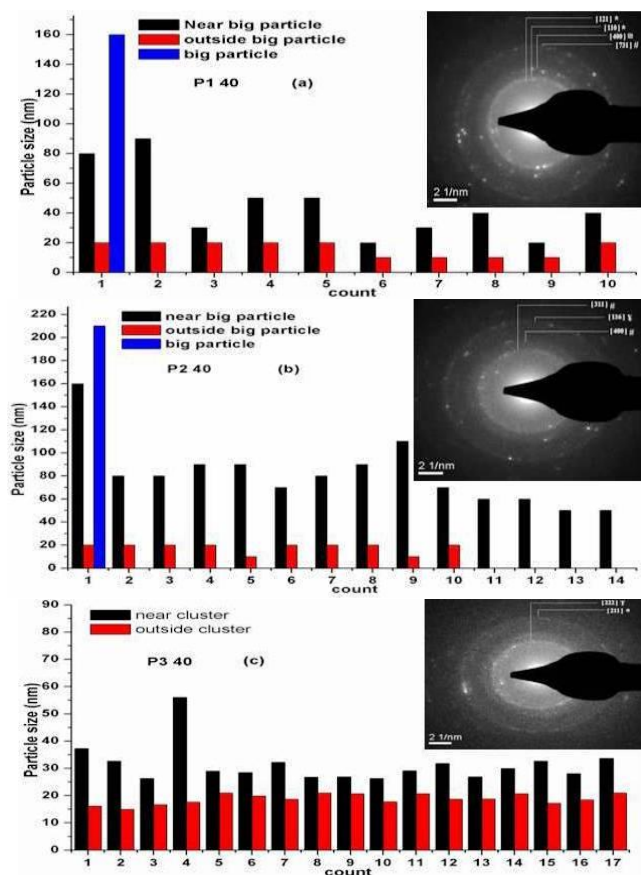
Histogram has been plotted on the basis of agglomerations of NPs near / outside the bigger particle. Ring pattern shown in the inset of **Fig. 7** (**a**) is due to diffraction from [121], [110] planes of Fe_2O_3, while [400] and [731] planes represent presence of titanomaghemite and pseudobrookite phases of titanium ferrite, which is also evidenced by XRD pattern (**Fig. 3**). In the inset of **Fig. 7** (**b**), planes [311], [400] corresponds to titanomaghemite, and [116] shows pseudobrookite phase. Similarly in the inset of **Fig. 7** (**c**), plane [222] shows ulvoespinel while [211] corresponds to Fe_2O_3 structure.

Fig. 8 shows TEM micrographs with corresponding EDX spectra of titanium ferrite NPs obtained from laser ablation of pellet P2 with varying laser pulse energy. TEM images [(**a**)-(**c**)] reveal that effects of laser pulse energy variations on degree of agglomeration is higher as compared to the variation of Ti/Fe ratio in target. **Fig. 9** (**a-c**) represents the particle size distributions of NPs produced with LP-PLA of target P2 at different laser pulse energies (40, 50, 60 mJ / pulse). Ring pattern, shown in the inset of **Fig. 9** (**a**), is already discussed in previous paragraph. Diffraction pattern of sample produced with LP-PLA of target P2 with 50 mJ/pulse energy (inset **Fig. 9** (**b**)), shows diffractions from [201] plane of pseudobrookite, [310] plane of titanomaghemite and [440] plane of shows Ti_3Fe_3O structure. SAED patterns support XRD results of presence of multiphasic structure in all titanium ferrite NPs samples [28].

Fig. 7 (**a-c**) Particles size distribution and SAED pattern (insets) of samples P1, P2 and P3. (Symbols in insets:-'*'→Fe₂O₃, '#'→titanomaghemite, '₪'→Ti₃Fe₃O, '¥' →pseudobrookite, 'Ŧ' → ulvoespinel).
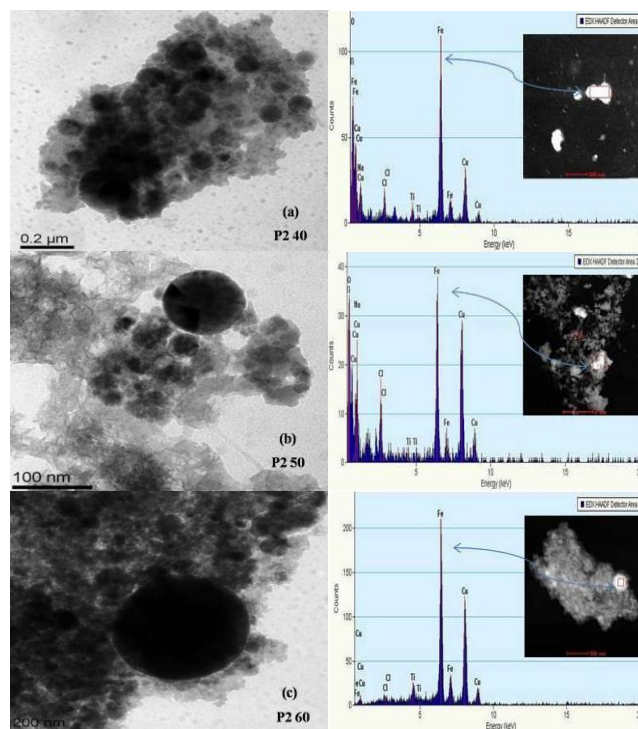

Fig. 8. TEM micrographs (a-c) with their EDX spectrum of sample P2 synthesized at different energies (40, 50 and 60 mJ).

Furthermore, the particle diameters are about 75, 18.54 and 54.86 nm near the agglomerated region while bigger particle diameters are about 210, 92 and 392 nm for samples produced with PLA of P2 followed by post-irradiation using 40, 50 and 60 mJ/pulse energy

respectively {**Fig. 9 (a-c)**}. Corresponding sizes of particles those are dispersed outside the agglomerated region are about 18, 9.33 and 16.01 nm (**Table. 1**). When laser pulse energy is varied from 40 to 60 mJ/ pulse, LIC phenomenon takes place which is correlated with the UV-visible results. It is clearly demonstrated from the bar graphs (**Fig. 7**) that PLA of target P2 with 50 mJ/pulse energy produces smallest size of titanium ferrite NPs. EDX patterns illustrate that iron composition is highest as compared to other elements in produced NPs.

Fig. 9 (a-c) Particles size distribution and SAED pattern (insets) of sample P2 synthesized at different energies (40, 50 and 60 mJ). (Symbols in insets:- '#'→titanomaghemite,'¥' →pseudobrookite, '₪'→Ti$_3$Fe$_3$O).

Magnetic characteristics of titanium ferrite NPs

The magnetic measurement is carried out with the help of hysteresis loop recorded at room temperature using VSM technique. The values of coercivity (Hc), saturation magnetization (Ms), and remanent magnetization (Mr) are determined from M-H loop. **Fig. 10** shows hysteresis loop of as synthesized samples produced with laser ablation followed by post irradiation of P1, P2, and P3 targets using 40 mJ/ pulse energy. The coercivity and other magnetic properties such as ferromagnetism have a direct relationship with the crystalline shapes and sizes of particles [**29**]. **Fig. 10** demonstrates that saturation magnetization (Ms) and remanence (Mr) have linear dependence on crystalline size, which predicts impregnation of TiO$_2$ at the interface of Fe$_2$O$_3$ matrix and pinning of the surface spins [**30**].
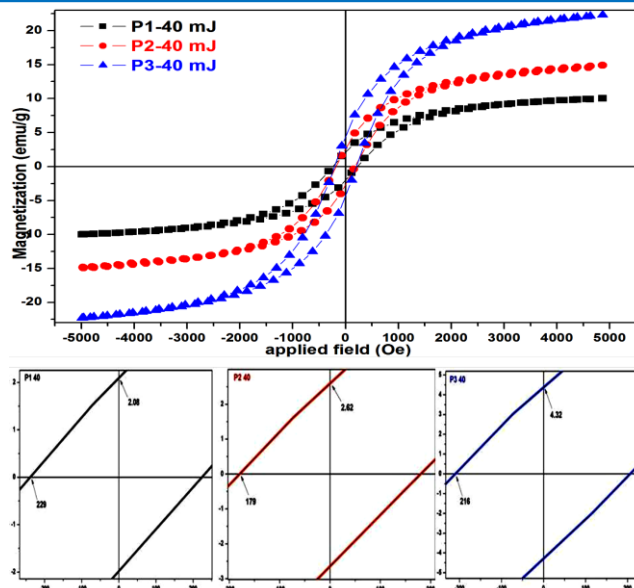

Fig. 10. M–H plots of samples P1, P2 and P3 NPs with their close inset around origin.

The coercivity of P1 at 40 mJ sample is maximum (229 Oe), while that of P2 at 40 mJ sample (179 Oe) is minimum. Saturation magnetization (22 emu/ g) and remanence (4.32 emu/ g) have highest values for sample P3 at 40 mJ, while these have least magnitudes for P1 40 mJ sample. Saturation magnetization and remanence have maximum values due to high ratio of Fe$_2$O$_3$ and TiO$_2$, where Fe$_2$O$_3$ shows magnetic character while TiO$_2$ blocks some of the magnetic sites [**31**]. **Fig. 11** shows M-H loop of sample P2 ablated at different energies (40, 50 and 60 mJ/ pulse) which doesn't demonstrate a large effect in their magnetic behavior.
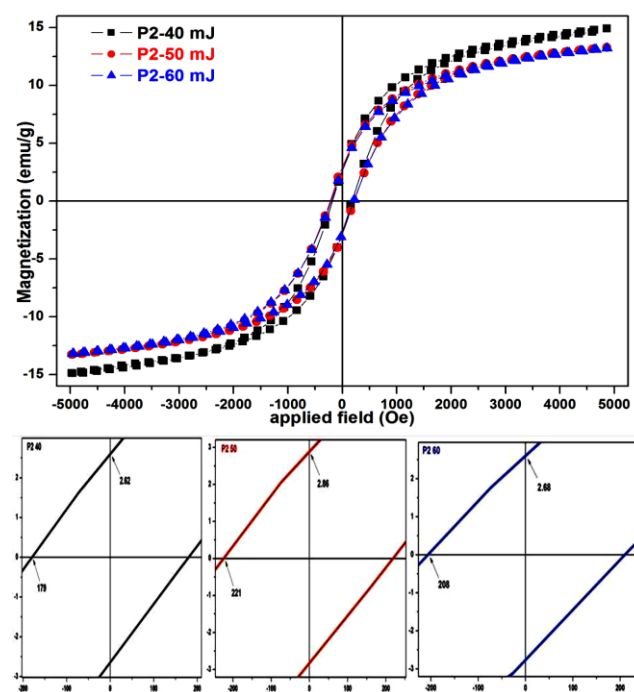

Fig. 11. M–H plots of samples P2 40, 50 and 60 NPs with their close insets around origin.

Conclusions

Titanium ferrite NPs are synthesized successfully using liquid-assisted pulsed laser ablation followed by post-irradiation treatment in doubled distilled water. Obtained results indicate that with the increase of titanium in the target material, optical band gap increases, while particle size, ferromagnetism, degree of spherical particles formation and rate of agglomeration/aggregation get decreased. It means that one has to choose higher Ti/Fe ratio in order to get smaller sized but less ferromagnetic NPs, and vice versa. Higher ferromagnetism with larger sized particles demonstrates dominance of bulk phenomenon over surface defects for the ferromagnetic responsible spins. Variation in laser pulse energy at a given Ti/Fe ratio does not show much effect on the optical band gap, size and magnetic properties of produced NPs. It reveals that titanium ferrite NPs can be used as photo catalyst in ultraviolet spectral region where titanium can alter magnetic properties in Fe_2O_3 lattice.

Reference

1. Thareja. R. K., Shukla. S., *J. Applied Surface Science*., **2007**, *253*, 8889.
   DOI: 10.1016/j.apsusc.2007.04.088
2. Bajaj. Geetika, Soni. R.K., J. *Appl Phys A*, **2009**, *97*, 481.
   DOI: 10.1007/s00339-009-5248-5
3. Yang. R, Chueh. Yu-Lun *et al*, *J. Nano. Lett*., **2007**, *7*, 269.
   DOI: 10.1021/nl062228b
4. Rakshit, R. K.; Sharma, R.; Budhani, R. C. *et al*, *J. Appl. Phy*., **2008**, *103*, 023915.
   DOI: 10.1063/1.2832763
5. Shahi. A. K.; Pandey. B. K., Pandey. J. K., Sinha. A. K., Gopal. R., *J. Mat. Foc.*, **2013**, *2*, 1.
   DOI: 10.1166/mat.2013.1100
6. Singh, S. C., and Gopal, R., *J. Phys. Chem. C*., **2008**, *112*, 2812.
   DOI: 10.1021/jp0753676
7. Pandey, B.K., Shahi, A.K., Gopal, R., *Applied Surface Science*., **2013**, *283*, 430.
   DOI: 10.1016/j.apsusc.2013.06.126
8. Niu, K.Y., Yang, Jing, Sun, Jing.; Du, Xi-Wen., *J. Nanotechnology*., **2010**, *21*, 295604.
   DOI: 10.1088/0957-4484/21/29/295604
9. Liu, Peisheng; Cai, Weiping and Zeng, Haibo; *J. Phys. Chem. C*., **2008**, *112*, 3261.
   DOI: 10.1021/jp709714a
10. Yang, S., Guo, Y., Yan, Naiqiang *et al*, *J. ACS Appl. Mater. Interfaces*. **2011**, *3*, 209.
    DOI: 10.1021/am100835c
11. Yang, Shijian, Guo, Yongfu, Yan, Naiqiang *et al*, *J. Chem. Commun*., **2010**, *46*, 8377.
    DOI: 10.1039/C0CC02645J
12. Tanga, H., Zhanga, Du, Tang, Guogang *et al*, *J. Ceramics International*., **2013**, *39*, 8633.
    DOI: 10.1016/j.ceramint.2013.04.040
13. Shi, J., Zheng, J., Hu, Y., and Zhao, Yu. **2008**, *49*, 279.
    DOI: 10.1134/S002315840802016X
14. Patel, M. N., Williams, Ryan D., Alan May, R. *et al*, *J. Chem. Mater.*, **2008** , *20*, 6029.
    DOI: 10.1021/cm8012705
15. Millot, N., Perriat, P., *J. Solid State Chem*., **2011**, *184*, 2776.
    DOI: 10.1016/j.jssc.2011.08.007
16. Pearce, C.I., Qafoku, O., Liu, J. *et al*, *J. Colloid and Interface Science*. **2012**, *387*, 24.
    DOI: 10.1016/j.jcis.2012.06.092
17. Sorescu, M., Xu, T., Wise, A. *et al*, *J. Mag. and Mag. Materials*., **2012**, *324*, 1453.
    DOI: 10.1016/j.jmmm.2011.12.012
18. Tanga, H.; Zhanga, D.; Tang, Guogang *et al*, *J. Ceramics International*., **2013**, *39*, 8633.
    DOI: 10.1016/j.ceramint.2013.04.040
19. deKrafft, K. E.; Wang, Cheng, and Lin *et al*, *J. Adv. Mater*., **2012**, *24*, 2014.
    DOI: 10.1002/adma.201200330
20. Thompson, T. L. and Yates, John T., Jr, *J. Chem. Rev.*, **2006**, *106*, 4428.
    DOI: 10.1021/cr050172k
21. Sivula, Kevin, Formal, Florian Le and Grtzel, Michael, *J. Chem Sus Chem*. **2011**, *4*, 432.
    DOI: 10.1002/cssc.201000416
22. Hirano, M., Joji, Toyoko & Inagaki, Michio, *J. Ant. Ceram. So.*,**2004**, *87*, 35.
    DOI: 10.1111/j.1151-2916.2004.tb19941.x
23. Wang, X. H., Li, J. G., Kamiyama, H. *et al*, *J. Am. Chem. Soc*., **2005**, *127*, 10982.
    DOI: 10.1021/ja051240n
24. Mafuné, F., Kohno. J., Takeda. Y. *et al*, *J. Phys. Chem. B*., **2000**, *104*, 8333.
    DOI: 10.1021/jp001803b
25. Mafuné, F., Kohno, J., Takeda, Y. *et al*, *J. Phys. Chem. B*., **2000**, *104*, 9111.
    DOI: 10.1021/jp001336y
26. Singh, S. C., Mishra, S. K., Gopal, R., *J. Phys. Chem. C.*, **2010**, *114*, 17374.
    DOI: 10.1021/jp105037w
27. Sorescu, M., Tarabasanu, D. M., Diamandescu, L., *J. Appl. Phys.*,**1999**, *85*, 5546.
    DOI: 10.1063/1.369890
28. Xu, Z., Huang. C., Wang, L., *J. Ind. Eng. Chem. Res*., **2015**, *54*, 4593.
    DOI: 10.1021/acs.iecr.5b00335
29. Selvan, R. K., Sanjeeviraja, C., D, Prabhakaran, *J. Solid State Comm.* **2006**, *137*, 512.
    DOI: 10.1016/j.ssc.2005.12.018
30. Wu, W., Xiao, X., Zhang, Shaofeng *et al*, *J. Nanoscale Research Lett*., **2011**, *6*, 533.
    DOI: 10.1186/1556-276X-6-533
31. Pandey, B. K., Shahi, A.K., Gopal, R *et al*, *J. Applied Surface Science*. **2014**, *289*, 462.
    DOI: 10.1016/j.apsusc.2013.06.126